

# The role of surface depletion layer effects on the enhancement of the UV emission in ZnO induced by a nanostructured Al surface coating.

*Saskia Fiedler\*<sup>1,2</sup>, Laurent O. Lee Cheong Lem<sup>1,3</sup>, Cuong Ton-That<sup>1</sup>, Matthew R. Phillips\*<sup>1</sup>*

Dr. Saskia Fiedler, Dr. Laurent O. Lee Cheong Lem, Assoc. Prof. Cuong Ton-That, Prof. Matthew R. Phillips

- <sup>1.</sup> School of Mathematical and Physical Sciences, University of Technology Sydney, 15 Broadway, Ultimo NSW 2007, Australia

Dr. Saskia Fiedler

- <sup>2.</sup> Centre for Nano Optics, University of Southern Denmark, Campusvej 55, 5230 Odense M, Denmark

Dr. Laurent O. Lee Cheong Lem

- <sup>3.</sup> Australian National Fabrication Facility, Australian National University, Canberra ACT 2601, Australia

E-mail: [safi@mci.sdu.dk](mailto:safi@mci.sdu.dk) and [matthew.phillips@uts.edu.au](mailto:matthew.phillips@uts.edu.au)

Keywords: Localized surface plasmons, cathodoluminescence, photoluminescence, ZnO, aluminum nanoparticles

## Abstract

The UV enhancement of Al-coated ZnO single crystals with a wide range of carrier densities is systematically studied using depth-resolved cathodoluminescence (CL) and photoluminescence (PL) as well as valence band X-ray photoemission spectroscopy (VB-XPS). An up to 17-fold enhanced PL UV emission for Al-coated ZnO with the highest carrier density ( $2 \times 10^{17} \text{ cm}^{-3}$ ) was measured, which falls to a 12-fold increase for the lowest carrier density ( $3 \times 10^{13} \text{ cm}^{-3}$ ). Depth-resolved CL measurements confirm that the enhancement is strongest near the metal coating – ZnO interface consistent with an increased UV emission due to an exciton – localised surface plasmon coupling mechanism. Correlative CL, PL and VB-XPS studies reveal that a number of additional effects related to the presence of the Al

surface coating also contribute to the UV enhancement factor. These include increased UV enhancement due to the formation of a surface depletion layer induced by the metal surface coating, which also passivates competitive non-radiative surface recombination channels found in uncoated ZnO. Significantly, it was established that the magnitude of the emission enhancement factor can be raised in a controlled way by reducing the thickness of the depletion layer by increasing the carrier density. The contribution of these effects collectively provides an explanation for the large span of enhancement factors reported in the literature.

## **Introduction**

Metal nanoparticle (NP) surface coatings can significantly enhance the excitonic luminescence of zinc oxide (ZnO) and other semiconductors [1–5] currently used in a broad array of applications in optoelectronics, photonics, photovoltaics and energy technologies. Here, a direct dipole-dipole coupling between the localized surface plasmons (LSPs) in the metal nanoparticles and the excitons in the ZnO creates an additional, non-radiative, faster relaxation channel via the LSPs, which subsequently leads to an increased spontaneous emission rate of the UV excitonic near band edge (NBE) emission [5,6]. This coupling mechanism is illustrated in fig. 1.

Gold (Au) and silver (Ag) are the most commonly used metal NPs for plasmonic applications. Although, Au NP coatings are relatively easy to fabricate as they are inert and stable, their plasmonic resonance is in the green spectral range, which makes Au films unsuitable for plasmonic coupling to the UV-excitons in ZnO [1,7,8]. Ag NPs, on the other hand, have their plasmon resonance in the blue/UV region; however, they readily form oxide and sulfur layers, which makes the fabrication of stable Ag NPs films difficult [9,10]. Conversely, Al NP films have a widely tunable plasmon resonance energy extending from the

UV to the visible spectrum, depending on the size and the shape of the NPs [11–14]. Even though Al NPs easily oxidize when exposed to air, the oxide layer thickness is typically self-limiting, which can be used to control the plasmon resonance energy [15]. Indeed, the UV excitonic emission in ZnO has been demonstrated to increase when the sample is coated with a surface film of Al NPs, which has been widely attributed to a mechanism involving exciton – LSP coupling. However, enhancement factors extending over a few orders of magnitude have been reported from samples that seem to be identical by their description [3,4,16–20], suggesting that there are additional effects contributing to the measured Al metal film induced increase in the light emission.

In this work, the UV enhancement of Al-coated ZnO single crystals with a wide range of carrier densities was systematically studied using photoluminescence (PL) spectroscopy and depth-resolved cathodoluminescence (CL). An up to 17-fold enhanced PL UV emission for Al-coated ZnO with the highest carrier density ( $2 \times 10^{17} \text{ cm}^{-3}$ ) was measured, which falls to a 12-fold increase for the lowest carrier density ( $3 \times 10^{13} \text{ cm}^{-3}$ ). Correlative CL, PL and valence band photoelectron X-ray spectroscopy (VB-XPS) measurements also reveal that a metal surface coating (i) passivates competitive non-radiative surface recombination channel present in the uncoated ZnO and (ii) creates a surface depletion layer, which both contribute to the magnitude of UV enhancement factor. The observed UV enhancement induced by the metal coating is accompanied by changes to the relative intensity of the defect-related deep level (DL) emission bands at the near surface, which is attributed to surface band bending that ionizes donors involved in competitive radiative recombination centers.

## **Methods**

The samples used in this study are polished *a*-plane ZnO single crystal 5 x 5 x 0.5 mm plates obtained from MTI Corporation USA, which were all carefully re-polished to an average surface roughness (RMS) of 1 nm. An identical polishing procedure was used every time to prevent any sample preparation induced variations in the specimens. A set of 5 samples was selected with carrier densities of  $3.0 \times 10^{13} \text{ cm}^{-3}$ ,  $1.8 \times 10^{14} \text{ cm}^{-3}$ ,  $2.7 \times 10^{14} \text{ cm}^{-3}$ ,  $3.1 \times 10^{16} \text{ cm}^{-3}$  and  $2.0 \times 10^{17} \text{ cm}^{-3}$ , which were determined using Hall probe measurements. The ZnO plates were sputter-coated with a 2 nm thick Al film. Only half of each sample was coated with Al to leave the uncoated side as a control and reference. Prior to coating, all samples were cleaned using a standard procedure consisting of the sonication for 20 minutes in acetone, then isopropyl alcohol and finally deionized water.

CL spectroscopy was performed in an FEI Quanta 200 SEM equipped with a Gatan CF302 continuous flow liquid helium cold stage. Light emitted from the sample was collected by a parabolic mirror and analyzed using an Ocean Optics QE Pro spectrometer. The parabolic mirror was also used to inject laser light focused at the sample plane and to collect PL, enabling direct spectral CL and PL measurements on spatially comparable regions of the samples. PL was excited with the 325 nm line of a Melles Griot He-Cd laser with varying powers from 0.1 to 3 mW. All luminescence spectra were corrected for the total response of the light collection system.

Depth-resolved CL spectra were collected at 3 kV, 5 kV, and 10 kV, providing probe depths of 40 nm, 100 nm and 350 nm below the surface, respectively, corresponding to the distance below the surface at which 70% of the integrated electron energy loss occurs, as determined by CASINO simulations [21]. In the depth-resolved measurements, the electron beam power was kept constant at 17.5  $\mu\text{W}$  at each voltage by varying the electron beam current to provide

the same number of injected electron-hole pairs at each acceleration voltage. At an acceleration voltage of 5 kV, the CL and PL excitation range can be considered to be comparable, assuming that the PL energy loss follows a Beer-Lambert relationship with depth  $z$ , being proportional to  $\exp(-\alpha z)$ , where  $\alpha$  is the absorption coefficient for ZnO at 325 nm. However, it is significant to note that the CL excitation density at 5 kV is approximately three orders of magnitude larger than the laser source as the lateral diameter of the CL excitation volume ( $\sim 0.040 \mu\text{m}$ ) is considerably smaller than the PL excitation spot diameter ( $30 \mu\text{m}$ ). Additionally, it is also important to note that although the excitation depth is similar for the PL and CL measurements at 5 kV, the energy loss profile of the laser is highest at the surface and then decays following the Beer-Lambert law. In contrast, the Monte Carlo simulations reveal that the CL in-depth energy loss profile versus kV has its maximum at a depth of approximately 20, 42 and 120 nm for electron beam energies of 3 kV, 5 kV, and 10 kV, respectively. This difference in the CL and PL in-depth energy loss arises because, unlike light, the energetic electrons must slow down via inelastic scattering mechanisms before they can strongly interact with the crystal lattice.

Hall effect measurements were carried using a conventional van der Pauw four-probe setup. VB-XPS was performed on the Soft X-ray Spectroscopy beam line at the Australian Synchrotron with an X-ray photon energy of 150 eV, which corresponds to a sampling depth of about 9 nm. A SPECS Phoibos 150 Hemispherical Analyzer was used for detection. All measurements were performed on the ZnO crystal with an intrinsic carrier density of  $2.7 \times 10^{14} \text{ cm}^{-3}$  (labeled sample 1), while a set of samples with varying carrier densities from  $1 \times 10^{13}$  to  $2 \times 10^{17} \text{ cm}^{-3}$  were studied with PL spectroscopy with laser excitation powers ranging from 0.1 to 3 mW.

## **Results**

VB-XPS was performed to characterize the surface band structure of a ZnO specimen (sample 1) with and without the Al coating. The results of the VB-XPS measurements are depicted in Fig. 2 (a), showing the Zn 3d peak at 10.2 eV and peaks near the valence band maximum centered at 7 eV and 5 eV, that are attributed to hybridized Zn 4s-O 2p states and O 2p states, respectively [23–27]. Fig. 2 (b) shows an enlargement of the valence band onset shown in Fig. 2 (a) around 3.0 eV. The magnitude of the surface band bending ( $V_{BB}$ ) can be determined using the following equation:

$$V_{BB} = E_g - E_{VF} - E_{CF}$$

Where,  $E_g = 3.37$  eV is the band gap of ZnO at room temperature,  $E_{VF}$  is the energy difference between the valence band maximum to the Fermi level at  $E = 0$ , which can be found from the intersection of the linear fits of the VB leading edge with the XPS background in Fig. 2 (b) and  $E_{CF}$  is the energy difference between the Fermi level and the conduction band minimum, with  $E_{CF} = (k_B T/e) \ln(N_C/n_e)$ , where  $k_B$  is the Boltzmann constant,  $N_C$  the effective density of states in the conduction band ( $2.94 \times 10^{18} \text{ cm}^{-3}$  for the effective mass of  $m_e^* = 0.24 m_e$ ),  $e$  is the elementary charge and  $n_e$  the bulk carrier density. Using the equation above, with the measured  $E_{VF}$  values from the  $n_e = 2.7 \times 10^{14} \text{ cm}^{-3}$ , reveals an upward surface band bending of + 0.20 V for the uncoated ZnO and a downward band bending at the surface of - 0.22 V for the Al NP coated ZnO. An upward band bending in the uncoated n-type ZnO is widely attributed to gaseous oxygen species being chemisorbed onto the top face, capturing free electrons from the bulk and creating a surface depletion layer [22,25,28]. The downward band bending measured from the Al NP coated sample is expected as the work function ( $\phi$ ) of

the Al (3.65-4.20 eV) is smaller than the electron affinity ( $\chi$ ) of n-type ZnO (4.5-4.7 eV) [29–32]. The resulting electron transfer from the metallic Al coating to the ZnO produces a surface accumulation layer, inducing downward band bending, consistent with the XPS VB measurements.

The width of the surface depletion layer ( $W$ ) and the surface electric field strength are both dependent on  $n_e$  and can be calculated using the following two equations [33]:

$$W = \sqrt{\frac{2\varepsilon_0\varepsilon_r V_{BB}}{qn_e}} \quad \text{and} \quad E_s = \frac{qn_e W}{\varepsilon_0\varepsilon_r},$$

where  $\varepsilon_0$  is the vacuum permittivity =  $8.85 \times 10^{-14}$  C/Vcm and  $\varepsilon_r = 8.66$  the relative permittivity of ZnO. Using these equations,  $W$  and  $E_s$  were determined using with  $V_{BB}$  values measured using the VB-PS results for the  $n_e = 2.7 \times 10^{14}$  cm<sup>-3</sup> sample. These results reveal a similar space charge layer width,  $W$ , of 840 nm and 880 nm and a corresponding electric field at the surface,  $E_s$ , of  $2.3 \times 10^3$  Vcm<sup>-1</sup> (out of the sample) and  $5.0 \times 10^3$  Vcm<sup>-1</sup> (into the sample) before and after coating, respectively. It is noteworthy that the electrostatic properties of the surface depletion layer of the uncoated and Al NP coated ZnO films are similar except for the opposite polarity of the surface electric field.

Fig. 3 (a) and (b) show the results of depth-resolved CL at 3 kV, 5 kV and 10 kV measured at 80 K, where the spectra with full and dashed lines are measured from the uncoated and Al coated sides of sample 1, respectively. The spectra consist of a UV emission around 3.37 eV from free exciton (FX) and bound exciton (BX) recombination as well as broad peak positioned at 2.1 eV related to defects and impurity centers, discussed below. The UV emission of the ZnO crystal with the Al surface coating is significantly enhanced at all excitation voltages as shown in Fig 3. (a). This UV enhancement is attributed to LSP-exciton coupling as the Al NP LSP resonance is in the UV spectral range, enabling a direct dipole-

dipole energy exchange with the excitons in the ZnO. The availability of this additional fast relaxation pathway increases the excitonic spontaneous emission rate, and consequently the CL intensity [3,5,6]. The largest UV enhancement of 8.3 is observed at the lowest acceleration voltage of 3 kV where excitons are excited near the Al/ZnO interface consistent with the LSP-exciton coupling mechanism. By increasing acceleration voltages to 5 kV and then 10 kV, the depth of maximum exciton excitation shifts away from the surface and accordingly the UV enhancement factor is reduced to 3.3 and 2.3, respectively.

The Al NP surface coating also modifies the DL CL emission as shown in Fig. 3 (b). Gaussian curve fitting of the DL from the single crystal ZnO shows that the broad emission consists of two peaks: a green luminescence (GL) peak at 2.3 eV and an orange luminescence (OL) at around 2.0 eV as seen in Fig. 3 (c)-(d) at an acceleration voltage of 3 kV and 10 kV, respectively. Comparative depth-resolved CL spectroscopy measurements of samples with and without Al NP surface film reveal that the Al coating quenches the GL and conversely increases the OL. The magnitude of these changes to the GL and OL is strongest near the surface at 3 kV (~ 40 nm), becoming progressively weaker at larger depths when the kV increases from 5 kV (~ 100 nm) to 10 kV (~ 350 nm). Both of these DL peaks have been attributed to radiative recombination at shallow donor – deep acceptor complexes. Here, the deep acceptor has been reported to be either substitutional lithium ( $\text{Li}_{\text{Zn}}$ ) or interstitial oxygen ( $\text{O}_i$ ) for the OL [34,35] and zinc vacancy ( $\text{V}_{\text{Zn}}$ ) related centers for the GL [36,37], while shallow donors include H, Zn and Li interstitials ( $\text{H}_i$ ,  $\text{Zn}_i$  and  $\text{Li}_i$ ) as well as substitutional Al ( $\text{Al}_{\text{Zn}}$ ). The Al surface coating induces a shallow donor  $0/+$  charge transition band to bend below the surface pinned Fermi level, ionizing a neutral shallow donor involved in the GL, switching its GL charge state, quenching the GL, and increasing the emission from the competitive deeper OL recombination channel [38,39]. This mechanism explains why the magnitude of the enhancement of the OL and quenching of the GL both decrease as the kV

becomes higher, because a larger number of electron hole pairs are injected at greater depths below the depletion layer, where the shallow donor charge state switching does not occur. The main point here is that the enhancement of the OL is not related to a coupling effect, which is expected because of the large difference in energy between the OL and Al LSP resonance. Note that the PL measurements of the before and after Al surface coated ZnO produce a similar UV enhancement to those described above acquired with CL excitation, including a similar change in DL as well (not shown).

The log-log plots of the CL and PL intensity versus CL and PL excitation power from  $n_e = 2.7 \times 10^{14} \text{ cm}^{-3}$  sample with and without an Al NP coating are shown for the PL UV NBE in Fig. 4 (a), PL DL in Fig. 4 (b), CL UV NBE in Fig. 4 (c) and for CL DL in Fig. 4 (d). Here, the integrated intensity of the UV NBE emission and the DL emission were measured between 3.00 to 3.45 eV and 1.20 to 3.00 eV, respectively. The results show that the integrated UV emission of the Al NP coated ZnO is higher than that of the uncoated side with both PL and CL excitation at all excitation powers. A linear fit of these log-log excitation power density plots provides a power law exponent,  $m$ , with  $\log I_{\text{CL/PL}} = m \log (P_{\text{ex}})$ . Here,  $m$  is either:  $m < 1$  (sub-linear) due to saturation of the defect,  $m = 1$  (linear) no saturation of the recombination channel, or  $m > 1$  typically arises from saturation of other competing radiative and non-radiative recombination pathways. Fig. 4 (a) shows that for the UV PL emission versus laser power, where  $m$  is super-linear ( $1.12 \pm 0.01$ ) for the uncoated ZnO and linear ( $1.04 \pm 0.01$ ) for the Al-coated side. The result strongly suggests that the Al coating passivates a competitive surface related recombination channel in the uncoated ZnO that saturates with increasing excitation power. The DL in uncoated ZnO exhibits a sub-linear power law exponent in Fig. 4 (b), indicating that these DL recombination pathways saturate with increasing beam power. This result is consistent with the slow relaxation lifetime of the GL [40], which is of the order of  $\mu\text{s}$  and much longer than that of the UV NBE emission

being typically tens or hundreds of ps [41,42]. Thus, the saturation of the slower competitive GL recombination channel with increasing excitation power leads to an increase of the significantly faster UV emission, explaining both the sub-linear power law exponent of the DL emission as well as the super-linear behavior of the UV emission of the uncoated ZnO. Conversely,  $m$  is linear for the DL emission from the Al-coated ZnO, since the Al surface coating quenches the GL due to the downward band bending as described above, leaving the OL, which exhibits a relatively faster relaxation time [40]. The CL excitation density dependence results are shown in Fig. 4 (c) and Fig. 4 (d). The CL power law exponent results are the same as the PL measurements, except for the uncoated DL CL data showing stronger saturation effects due to the higher injected electron hole pair density with CL compared to PL excitation.

The NBE enhancement factor dependence on excitation power at 10 K, 80 K and 300 K using sample 1 with and without an Al surface coating is shown in Fig. 5 (a) and 5 (b) for CL and PL, respectively. The maximum UV enhancement is found at the lowest excitation power of both the electron beam and the laser. This observation can be explained using the results in Fig. 4 (a) and Fig. 4 (c), which reveal that UV emission intensity of the uncoated ZnO increases super-linearly with increasing excitation power while on the Al-coated side it scales linearly. Consequently, the NBE enhancement factor, being the ratio of these two intensities, will decrease with increasing excitation power due to the super-linear and linear power-law exponents exhibited by the ZnO samples with and without an Al coating, respectively.

To investigate the effect of the intrinsic carrier density in ZnO on the Al coating induced UV enhancement factor, power dependent PL spectroscopy was conducted on five samples with carrier densities of  $3.0 \times 10^{13} \text{ cm}^{-3}$ ,  $1.8 \times 10^{14} \text{ cm}^{-3}$ ,  $2.7 \times 10^{14} \text{ cm}^{-3}$ ,  $3.1 \times 10^{16} \text{ cm}^{-3}$  and

$2.0 \times 10^{17} \text{ cm}^{-3}$ . The UV PL enhancement as a function of  $n_e$  and laser power, shown in Fig. 6, reveal that the UV enhancement factor increases with increasing  $n_e$ . Significantly, this result also shows that the strength of the emission enhancement factor can be controlled by varying  $n_e$ . However, the interpretation of these data requires inspection of the UV PL intensity versus  $n_e$  data for the sample with and without the Al surface coating that are shown in Fig. 7. The results from the uncoated ZnO sample show that the UV PL intensity decreases linearly with increasing  $n_e$  due most likely to the formation of additional competitive exciton recombination channels involving Auger relaxation processes. This explanation is supported by the excitation power dependence results displayed in Fig. 6 that reveal that the UV enhancement factor decreases with escalating laser power and that this effect becomes more pronounced with increasing  $n_e$ . Conversely, the decrease in UV PL in the uncoated sample with increasing  $n_e$  is not observed in the Al coated specimen as shown in Fig. 7. The surface Al coating, as shown and discussed above, can increase the UV PL by quenching competitive non-radiative surface recombination. However, this effect is independent of  $n_e$  and consequently cannot explain the increase in the PL emission, indicating that other phenomena in the bulk must contribute to the measured enhancement.

The VB-XPS results shown in Fig. 2 exhibit that the Al coating creates a surface depletion layer, which can be used to explain the absence of the decrease in the PL UV emission that is observed in the uncoated sample with rising  $n_e$ . For the sample with the lowest  $n_e$  ( $2 \times 10^{13} \text{ cm}^{-3}$ ), the width of the depletion region is calculated to be  $\sim 3,095 \text{ nm}$ , while for the highest  $n_e$  ( $1 \times 10^{17} \text{ cm}^{-3}$ ) it is considerably smaller, being  $\sim 44 \text{ nm}$ , noting that  $\sim 70\%$  of the PL excitation occurs within a depth of  $100 \text{ nm}$ . For these two samples, the corresponding surface electric field of Al-coated ZnO crystals is  $\sim 1.4 \times 10^3 \text{ Vcm}^{-1}$  and  $9.6 \times 10^4 \text{ Vcm}^{-1}$ , respectively, indicating an increase of approximately two orders of magnitude. Significantly

FX are stable in ZnO, despite the presence of these large surface electric fields. This is because of the large binding energy ( $E_x$ ) of FX in ZnO ( $E_x = 60$  meV) and their small Bohr radius ( $r_x = 2.3$  nm) [43,44]. Using these FX properties, the estimated electric field required to dissociate an FX in ZnO is  $\sim 2.6 \times 10^5$  Vcm<sup>-1</sup> ( $= E_x / q.r_x$ ) [45], which is higher than the maximum electric fields observed at the ZnO surface.

The presence of the surface depletion layer increases the measured UV emission in the Al coated ZnO via two effects. First, since there are no free carriers in the depletion region, the measured UV emission is enhanced owing to: (i) the removal of competitive Auger recombination pathways and (ii) a decrease in electron – exciton scattering, causing an increase in exciton diffusion length, increasing the strength of the FX-LSP coupling. Second, as the magnitude of the surface band bending increases as  $n_e$  becomes larger deeper competitive neutral donor recombination are ionized and consequently the UV emission is increased.

Fig. 6 also reveals that as the  $n_e$  increases in the n-type ZnO the UV enhancement factor becomes increasingly inversely dependent on the PL excitation power. Consequently, this reduction with power density is most pronounced with the highest  $n_e$  ( $1 \times 10^{17}$  cm<sup>-3</sup>) sample, where the UV enhancement factor decrease from 17 to 12 with an increasing laser excitation power from 0.1 to 2.1 mW, respectively, while at the lowest  $n_e$  ( $2 \times 10^{13}$  cm<sup>-3</sup>) the reduction of the enhancement factor is negligible. Given that the FX diffusion length in ZnO is  $\sim 200$  nm [46], this behavior is likely due to the creation of additional excess carrier related non-radiative relaxation channels in the bulk with increasing  $n_e$ . These are most likely competitive Auger recombination mechanisms at depths below the surface depletion layer

that quench the FX emission as well as limiting their diffusion towards the Al metal coating – ZnO interface.

### Conclusion:

Following the deposition of a 2 nm Al surface coating on an *a*-plane n-type ZnO with an  $n_e$  of  $2.7 \times 10^{14} \text{ cm}^{-3}$ , the UV PL and CL significantly increases with its maximum close to the surface. An up to 17-fold increase was observed in the PL excited UV NBE from the Al coated n-type ZnO. Depth-resolved CL analysis confirms that enhanced UV emission is due to an increase in the spontaneous emission rate due to the availability on an additional fast relaxation channel involving an LSP-exciton dipole-dipole coupling mechanism. However, correlative PL, CL and VB-XPS studies revealed that a number of other processes induced by the Al coating also contribute to the total UV emission enhancement, involving (i) the formation of a surface depletion region and (ii) quenching of surface recombination channels that are present in uncoated ZnO. The results also show that the strength of the optical emission enhancement factor can be increased and regulated by decreasing the thickness of the surface depletion layer by raising the carrier density of the ZnO. Furthermore, the presence of the surface depletion layer provides a highly likely explanation for the large span of enhancement factors reported in the literature, where their effects on the optical emission were not considered. The Al coating induced increased UV ZnO emission is accompanied by changes in the ZnO deep level emission that are attributed to surface band bending, ionizing shallow donors involved in competitive radiative recombination centers.

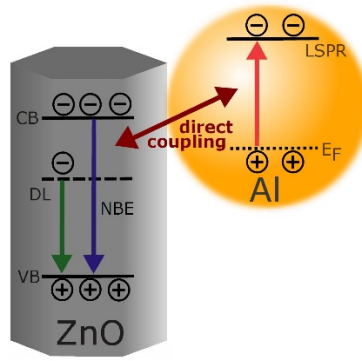


Fig. 1: Illustration of the LSP-exciton coupling mechanism.

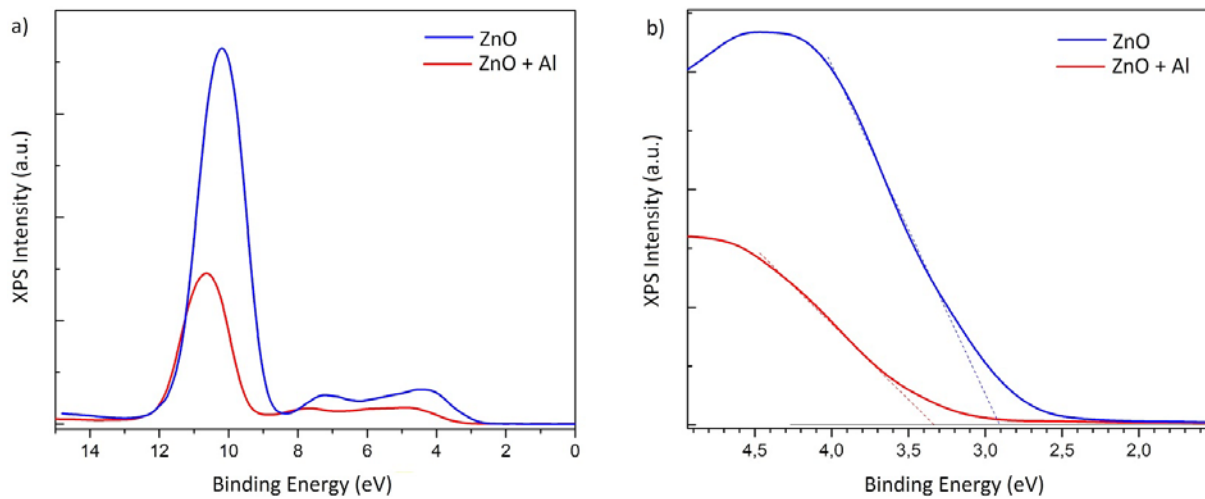


Fig. 2: (a) Valence band spectra of the uncoated (blue) and Al-coated a-plane ZnO (red) with a carrier density of  $2.7 \times 10^{14} \text{ cm}^{-3}$ . (b) Enlargement of the leading edge of valence band in (a) around 3.5 eV. The VB onset energy position is measured at the intersection of the linear fits of the VB leading edge and the background.

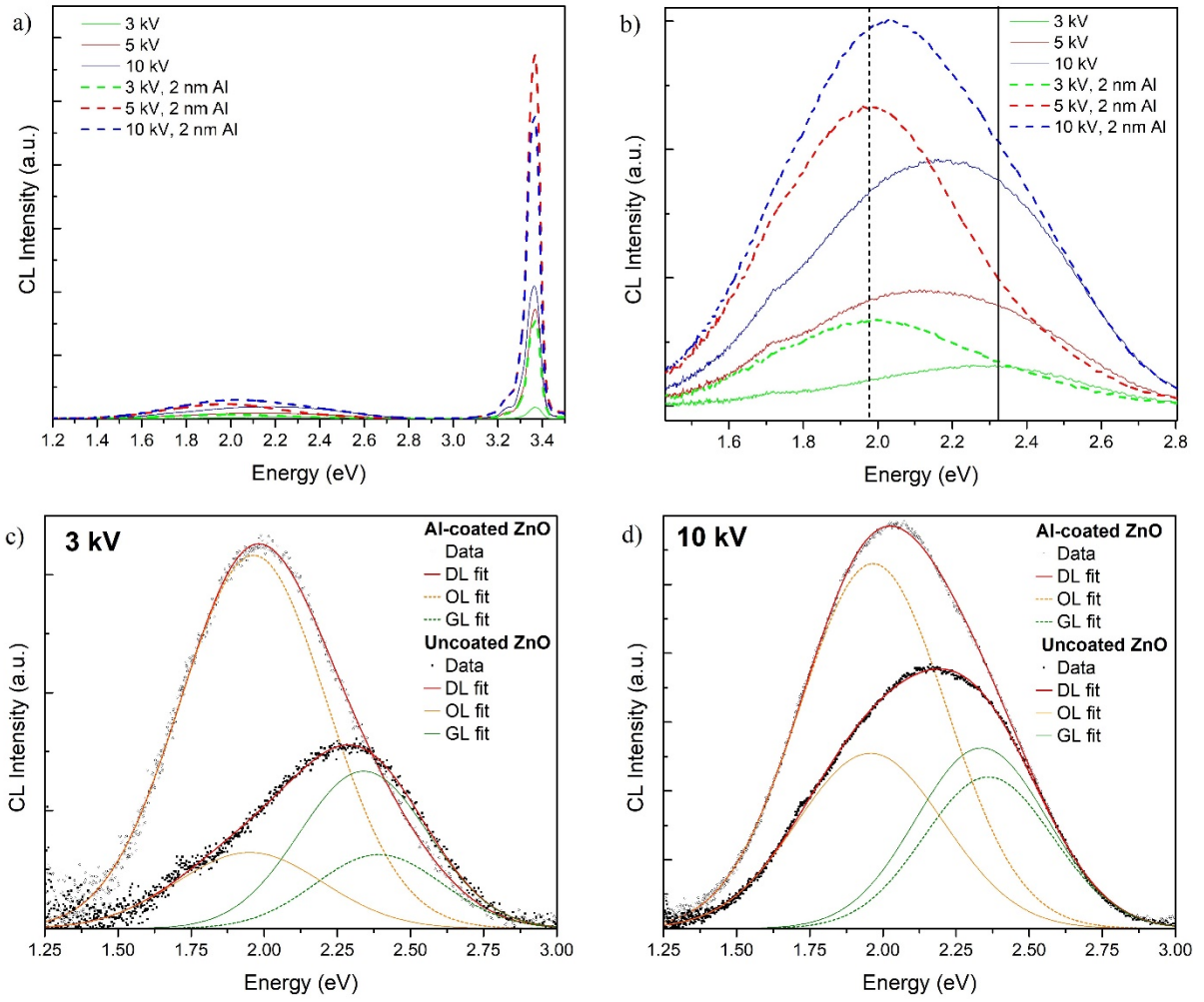


Fig. 3: (a) Depth-resolved CL spectra of uncoated (solid) and Al NP coated (dashed) *a*-plane ZnO (carrier density  $2.7 \times 10^{14} \text{ cm}^{-3}$ ) at  $T = 80 \text{ K}$ , showing highest UV enhancement of 8.3 at accelerating voltage of 3 kV. The spectra were collected with a constant electron beam power of  $17.5 \mu\text{W}$  and from a scan area of  $10 \mu\text{m} \times 10 \mu\text{m}$ . (b) Enlargement of the DL emission around 2.1 eV in (a), showing an increase in the CL emission at around 2.0 eV. (c) and (d) DL emission and fitting of the orange (OL) and green luminescence (GL) of the uncoated and Al-coated ZnO at 3 kV and 10 kV, respectively, showing a decreased GL and increased OL for the Al-coated ZnO.

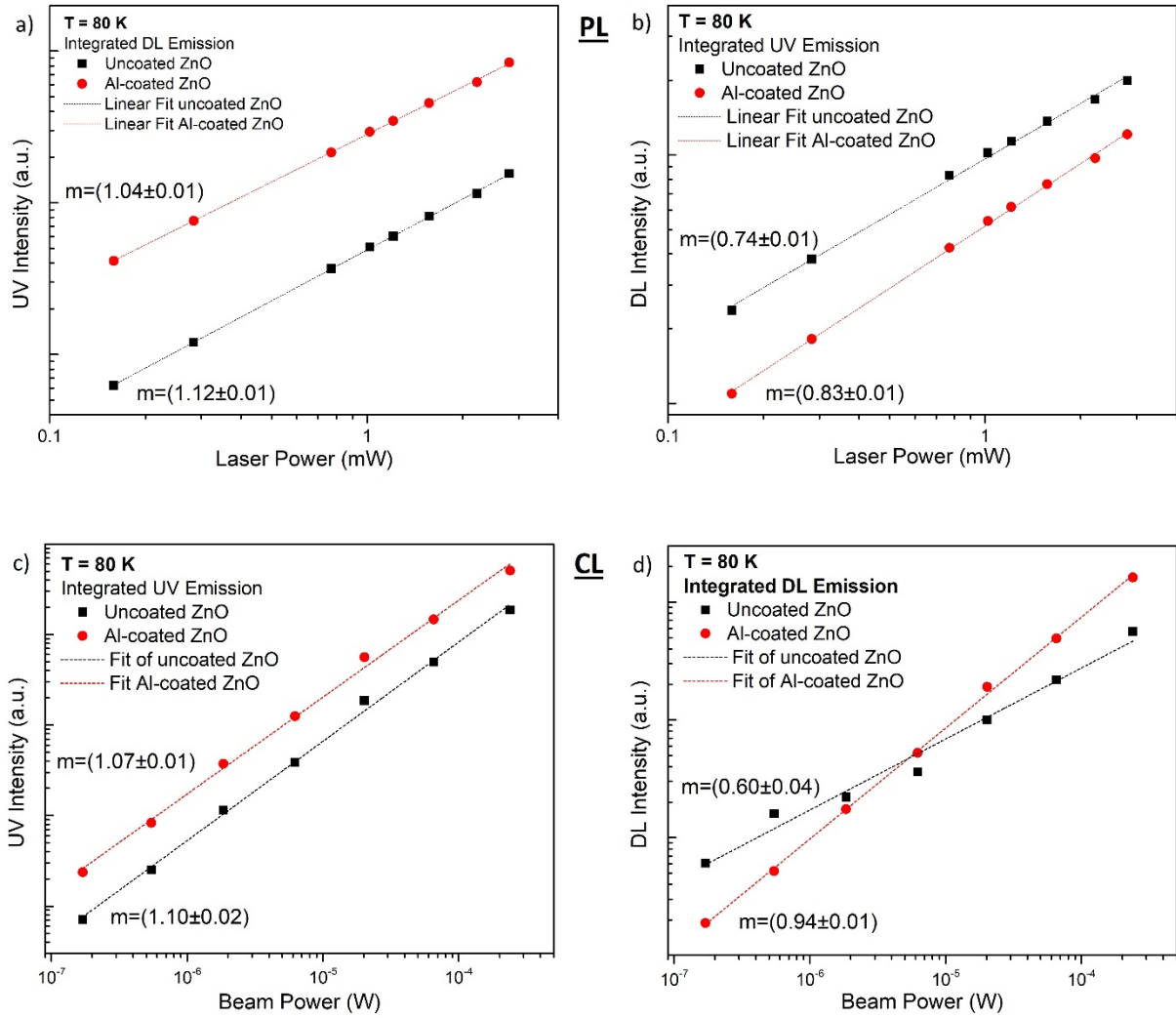


Fig. 4: Power-dependent PL of (a) the integrated NBE emission (3.00 - 3.54 eV) and (b) the DL emission (1.2 - 3.0 eV) of the uncoated (black) and Al-coated (red) ZnO with a carrier density of  $2.7 \times 10^{14} \text{ cm}^{-3}$ . (c) and (d) show the corresponding power-dependent CL, graphed logarithmically. PL: excitation = 325 nm, spot size  $\sim 30 \mu\text{m}$ ; CL: HV = 5 kV, scan area =  $15 \mu\text{m} \times 15 \mu\text{m}$ ; T = 80 K.

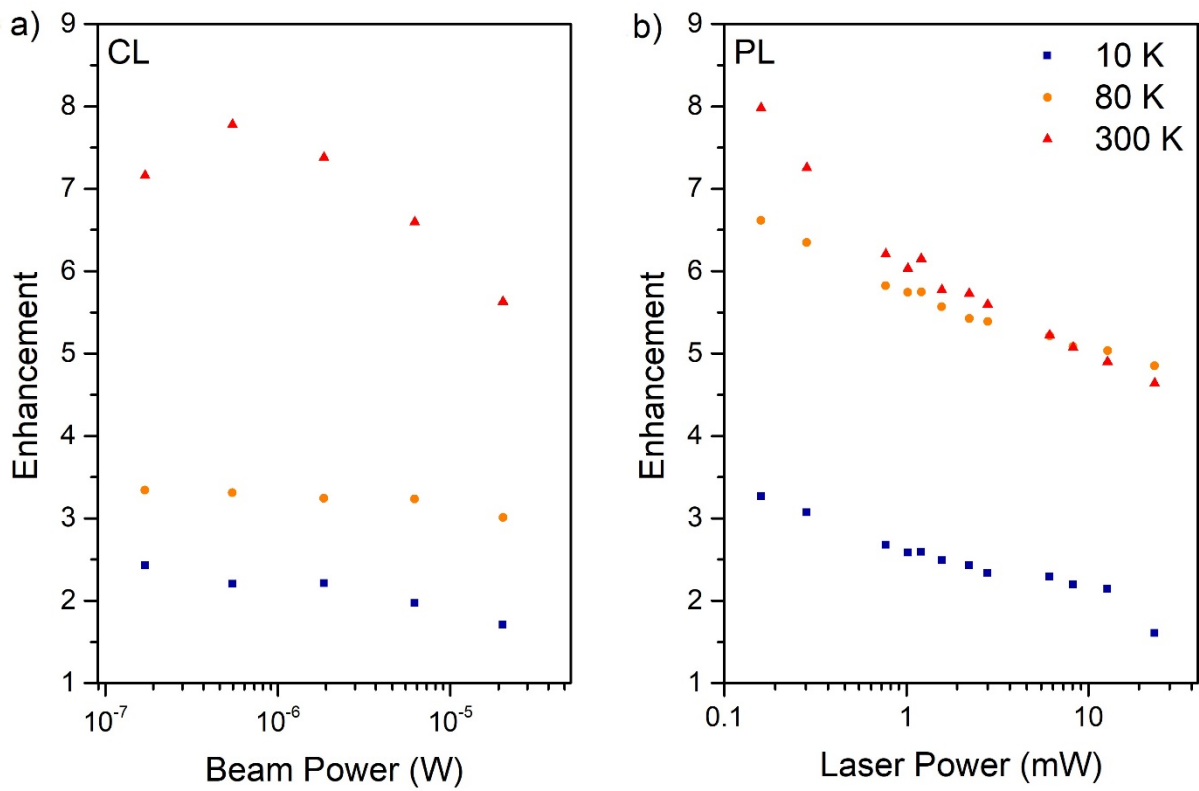


Fig. 5: (a) CL and (b) PL UV enhancement factor as a function of CL and PL excitation power from sample with an intrinsic carrier density of  $2.7 \times 10^{14} \text{ cm}^{-3}$  at temperatures of 10, 80 and 300 K.

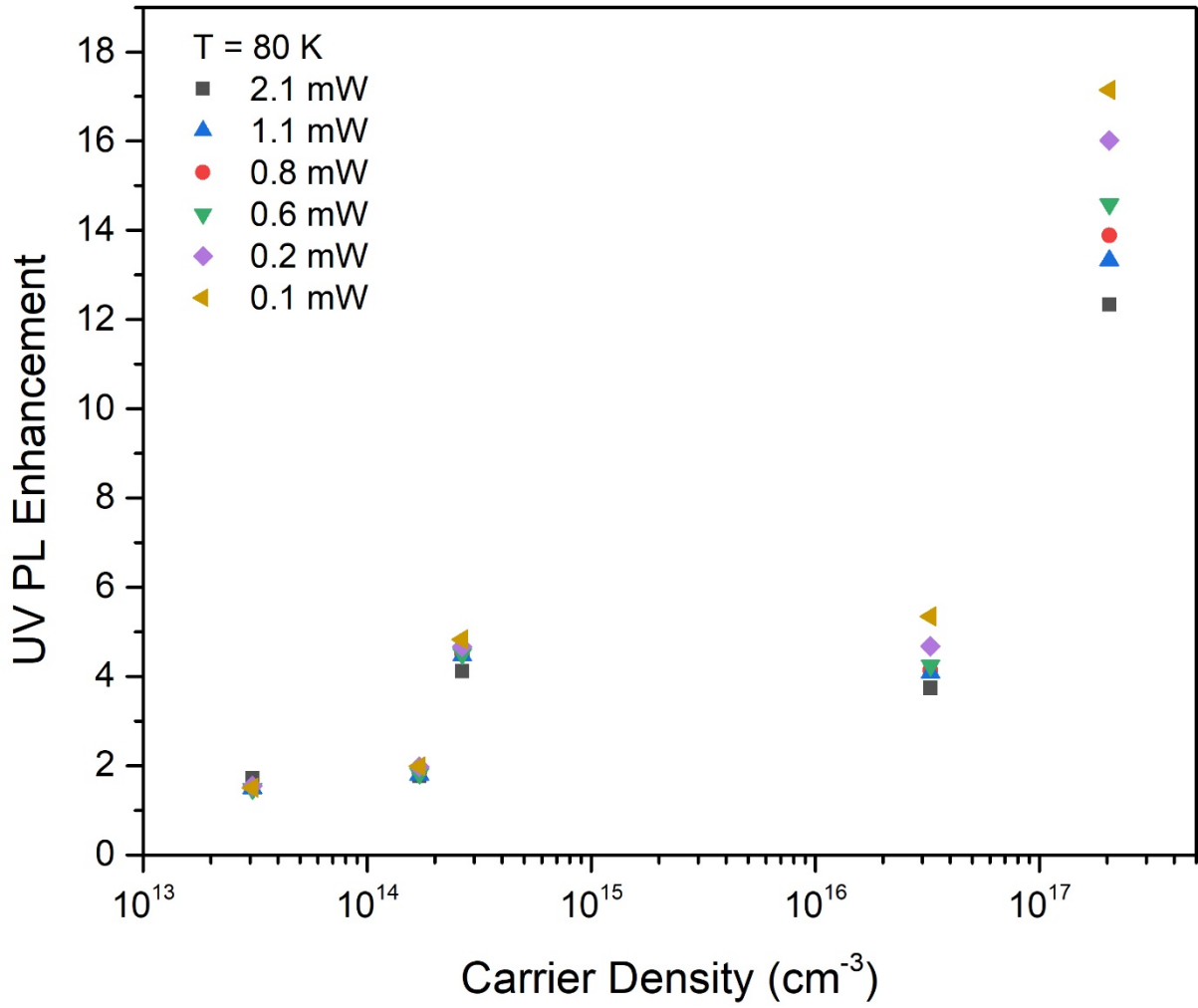


Fig. 6: UV enhancement of Al-coated *a*-plane n-type ZnO with different carrier densities ranging from  $10^{13}$  to  $10^{17}$   $\text{cm}^{-3}$ . The laser excitation power was varied from 0.1 mW to 2.1 mW at a wavelength of 325 nm with a spot size of  $\sim 30$   $\mu\text{m}$ .

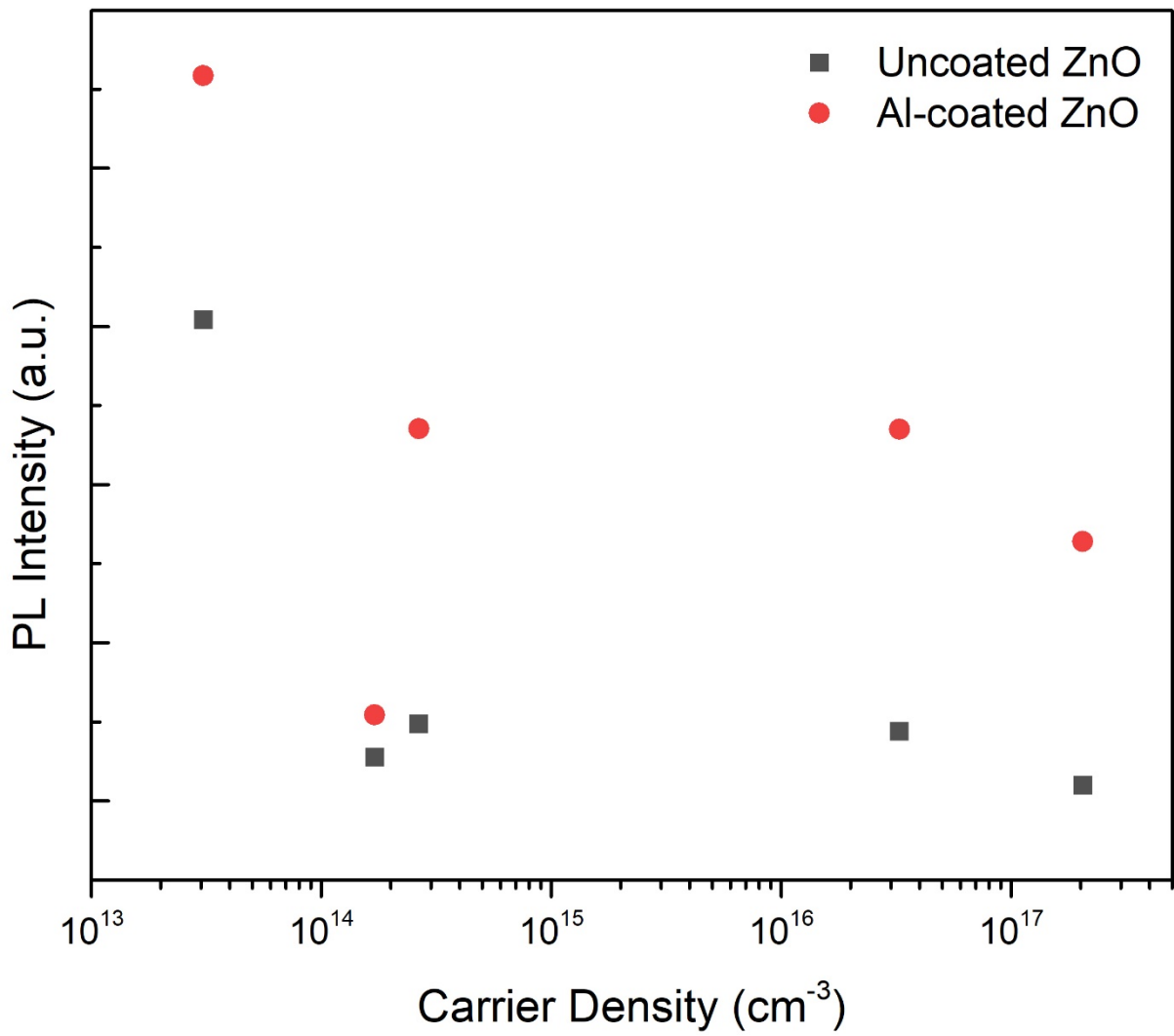


Fig. 7: PL Intensity before and after Al coating versus carrier density,  $n_e$  ( $\text{cm}^{-3}$ ). The uncoated sample exhibits a linear decrease in the PL intensity with increase  $n_e$ , which is absent in the coated sample due to the presence of a surface depletion layer, where its thickness decreases with increasing  $n_e$ .

## References.

1. Cheng, C.W., Sie, E.J., Liu, B., Huan, C.H.A., Sum, T.C., Sun, H.D., and Fan, H.J. (2010) Surface plasmon enhanced band edge luminescence of ZnO nanorods by capping Au nanoparticles. *Appl. Phys. Lett.*, **96** (7), 071107.
2. Zhang, Y., Li, X., and Ren, X. (2009) Effects of localized surface plasmons on the photoluminescence properties of Au-coated ZnO films. *Opt. Express*, **17** (11), 8735–8740.
3. Lu, J., Li, J., Xu, C., Li, Y., Dai, J., Wang, Y., Lin, Y., and Wang, S. (2014) Direct Resonant Coupling of Al Surface Plasmon for Ultraviolet Photoluminescence Enhancement of ZnO Microrods. *ACS Appl. Mater. Interfaces*, **6** (20), 18301–18305.
4. Lu, J., Xu, C., Dai, J., Li, J., Wang, Y., Lin, Y., and Li, P. (2015) Improved UV photoresponse of ZnO nanorod arrays by resonant coupling with surface plasmons of Al nanoparticles. *Nanoscale*, **7** (8), 3396–3403.
5. Ren, Q.J., Filippov, S., Chen, S.L., Devika, M., Koteeswara Reddy, N., Tu, C.W., Chen, W.M., and Buyanova, I.A. (2012) Evidence for coupling between exciton emissions and surface plasmon in Ni-coated ZnO nanowires. *Nanotechnology*, **23** (42), 425201.
6. Zang, Y., He, X., Li, J., Yin, J., Li, K., Yue, C., Wu, Z., Wu, S., and Kang, J. (2013) Band edge emission enhancement by quadrupole surface plasmon–exciton coupling using direct-contact Ag/ZnO nanospheres. *Nanoscale*, **5** (2), 574–580.
7. Su, L., and Qin, N. (2015) A facile method for fabricating Au-nanoparticles-decorated ZnO nanorods with greatly enhanced near-band-edge emission. *Ceram. Int.*, **41**, 2673–2679.
8. Pescaglioni, A., Martín, A., Cammi, D., Juska, G., Ronning, C., Pelucchi, E., and Iacopino, D. (2014) Hot-Electron Injection in Au Nanorod–ZnO Nanowire Hybrid Device for Near-Infrared Photodetection. *Nano Lett.*, **14** (11), 6202–6209.
9. Hillman, C., Arnold, J., Binfield, S., Seppi, J., and Park, C. (2007) Silver and Sulfur: Case Studies, *SMTA Inter.* 13.
10. Erol, M., Han, Y., Stanley, S.K., Stafford, C.M., Du, H., and Sukhishvili, S. (2009) SERS Not To Be Taken for Granted in the Presence of Oxygen. *J. Am. Chem. Soc.*, **131** (22), 7480–7481.
11. Knight, M.W., Liu, L., Wang, Y., Brown, L., Mukherjee, S., King, N.S., Everitt, H.O., Nordlander, P., and Halas, N.J. (2012) Aluminum Plasmonic Nanoantennas. *Nano Lett.*, **12** (11), 6000–6004.
12. Gérard, D., and Gray, S.K. (2015) Aluminium plasmonics. *J. Phys. Appl. Phys.*, **48** (18), 184001.
13. Langhammer, C., Schwind, M., Kasemo, B., and Zorić, I. (2008) Localized Surface Plasmon Resonances in Aluminum Nanodisks. *Nano Lett.*, **8** (5), 1461–1471.
14. Taguchi, A., Saito, Y., Watanabe, K., Yijian, S., and Kawata, S. (2012) Tailoring plasmon resonances in the deep-ultraviolet by size-tunable fabrication of aluminum nanostructures. *Appl. Phys. Lett.*, **101** (8), 081110.
15. Cabrera, N., and Mott, N. F. (1949) Theory of the Oxidation of Metals. *Rep. Prog. Phys.* **12** 163.
16. Zhang, H., Su, X., Wu, H., and Liu, C. (2019) Surface plasmon-enhanced UV-emission from ZnO by aluminum bowtie nanoantenna arrays. *J. Alloys Compd.*, **772**, 460–464.
17. Ding, X., Fang, Y., Zhao, M., Wang, W., Sha, J., and Wang, Y. (2017) Influence of Al capping on the photoluminescence of ZnO. *Opt. Mater. Express*, **7** (6), 1898.
18. Wu, K., Lu, Y., He, H., Huang, J., Zhao, B., and Ye, Z. (2011) Enhanced near band edge emission of ZnO via surface plasmon resonance of aluminum nanoparticles. *J. Appl. Phys.*, **110** (2), 023510.
19. Ni, W.H., An, J., Lai, C.W., Ong, H.C., and Xu, J.B. (2006) Emission enhancement from metallodielectric-capped ZnO films. *J. Appl. Phys.*, **100** (2), 026103.
20. Dellis, S., Kalfagiannis, N., Kassavetis, S., Bazioti, C., Dimitrakopoulos, G.P., Koutsogeorgis, D.C., and Patsalas, P. (2017) Photoluminescence enhancement of ZnO via coupling with surface plasmons on Al thin films. *J. Appl. Phys.*, **121** (10), 103104.

21. Drouin, D., Couture, A.R., Joly, D., Tastet, X., Aimez, V., and Gauvin, R. (2007) CASINO V2.42—A Fast and Easy-to-use Modeling Tool for Scanning Electron Microscopy and Microanalysis Users. *Scanning*, **29** (3), 92–101.
22. Anantachaisilp, S., Smith, S.M., Ton-That, C., Pornsuwan, S., Moon, A.R., Nenstiel, C., Hoffmann, A., and Phillips, M.R. (2015) Nature of red luminescence in oxygen treated hydrothermally grown zinc oxide nanorods. *J. Lumin.*, **168**, 20–25.
23. Chiou, J.W., Ray, S.C., Tsai, H.M., Pao, C.W., Chien, F.Z., Pong, W.F., Tseng, C.H., Wu, J.J., Tsai, M.-H., Chen, C.-H., Lin, H.J., Lee, J.F., and Guo, J.-H. (2011) Correlation between Electronic Structures and Photocatalytic Activities of Nanocrystalline-(Au, Ag, and Pt) Particles on the Surface of ZnO Nanorods. *J. Phys. Chem. C*, **115** (6), 2650–2655.
24. Ton-That, C., Phillips, M.R., Foley, M., Moody, S.J., and Stampfl, A.P.J. (2008) Surface electronic properties of ZnO nanoparticles. *Appl. Phys. Lett.*, **92** (26), 261916.
25. Allen, M.W., Zemlyanov, D.Y., Waterhouse, G.I.N., Metson, J.B., Veal, T.D., McConville, C.F., and Durbin, S.M. (2011) Polarity effects in the x-ray photoemission of ZnO and other wurtzite semiconductors. *Appl. Phys. Lett.*, **98** (10), 101906.
26. Chen, C.-Y., Retamal, J.R.D., Wu, I.-W., Lien, D.-H., Chen, M.-W., Ding, Y., Chueh, Y.-L., Wu, C.-I., and He, J.-H. (2012) Probing Surface Band Bending of Surface-Engineered Metal Oxide Nanowires. *ACS Nano*, **6** (11), 9366–9372.
27. Lin, Y., Wang, D., Zhao, Q., Li, Z., Ma, Y., and Yang, M. (2006) Influence of adsorbed oxygen on the surface photovoltage and photoluminescence of ZnO nanorods. *Nanotechnology*, **17** (9), 2110–2115.
28. Lord, A.M., Maffei, T.G., Allen, M.W., Morgan, D., Davies, P.R., Jones, D.R., Evans, J.E., Smith, N.A., and Wilks, S.P. (2014) Surface state modulation through wet chemical treatment as a route to controlling the electrical properties of ZnO nanowire arrays investigated with XPS. *Appl. Surf. Sci.*, **320**, 664–669.
29. Yacobi, B.G. (2003) *Semiconductor Materials: An Introduction to Basic Principles*, Springer Science & Business Media.
30. Lang, N.D., and Kohn, W. (1971) Theory of Metal Surfaces: Work Function. *Phys. Rev. B*, **3** (4), 1215–1223.
31. Mitchell Edgar William John, Mitchell John Wesley, and Mott Nevill Francis (1951) The work functions of copper, silver and aluminium. *Proc. R. Soc. Lond. Ser. Math. Phys. Sci.*, **210** (1100), 70–84.
32. Sundaram, K.B., and Khan, A. (1997) Work function determination of zinc oxide films. *Journal of Vacuum Science & Technology A*, **15**, 428.
33. Sze, S. M., and Ng, K.S. (2007) *Physics of Semiconductor Devices*.
34. Reshchikov, M.A., Garbus, J., Lopez, G., Ruchala, M., Nemeth, B., and Nause, J. (2006) Acceptors in ZnO Studied by Photoluminescence. *MRS Online Proc. Libr. Arch.*, **957**.
35. Børseth, T.M., Svensson, B.G., Kuznetsov, A.Yu., Klason, P., Zhao, Q.X., and Willander, M. (2006) Identification of oxygen and zinc vacancy optical signals in ZnO. *Appl. Phys. Lett.*, **89** (26), 262112.
36. Reshchikov, M.A., Xie, J.Q., Hertog, B., and Osinsky, A. (2008) Yellow luminescence in ZnO layers grown on sapphire. *J. Appl. Phys.*, **103** (10), 103514.
37. Ton-That, C., Weston, L., and Phillips, M.R. (2012) Characteristics of point defects in the green luminescence from Zn- and O-rich ZnO. *Phys. Rev. B*, **86** (11).
38. Rahman, M.A., Westerhausen, M.T., Nenstiel, C., Choi, S., Hoffmann, A., Gentle, A., Phillips, M.R., and Ton-That, C. (2017) Charge state switching of Cu acceptors in ZnO nanorods. *Appl. Phys. Lett.*, **110** (12), 121907.
39. Wang, D., and Reynolds, N. (2012) Photoluminescence of Zinc Oxide Nanowires: The Effect of Surface Band Bending. *ISRN Condens. Matter Phys.*, 1–6.
40. Reshchikov, M.A., Morkoc, H., Nemeth, B., Nause, J., Xie, J., Hertog, B., and Osinsky, A. (2007) Luminescence properties of defects in ZnO. *Phys. B*, **401–402**, 358–361.

41. van Dijken, A., Meulenkaamp, E.A., Vanmaekelbergh, D., and Meijerink, A. (2000) The Kinetics of the Radiative and Nonradiative Processes in Nanocrystalline ZnO Particles upon Photoexcitation. *J. Phys. Chem. B*, **104** (8), 1715–1723.
42. Travnikov, V.V., Freiberg, A., and Savikhin, S.F. (1990) Surface excitons in ZnO crystals. *J. Lumin.*, **47**, 107–112.
43. Özgür, Ü., Alivov, Ya.I., Liu, C., Teke, A., Reshchikov, M.A., Doğan, S., Avrutin, V., Cho, S.-J., and Morkoç, H. (2005) A comprehensive review of ZnO materials and devices. *J. Appl. Phys.*, **98** (4), 041301.
44. Klingshirn, C.F., Meyer, B.K., Waag, A., Hoffmann, A., and Geurts, J. (2010) *Zinc Oxide*, Springer Berlin Heidelberg, Berlin, Heidelberg.
45. Blossey, D.F. (1971) Wannier Exciton in an Electric Field. II. Electroabsorption in Direct-Band-Gap Solids. *Phys. Rev. B*, **3** (4), 1382–1391.
46. Noltemeyer, M., Bertram, F., Hempel, T., Bastek, B., Polyakov, A., Christen, J., Brandt, M., Lorenz, M., and Grundmann, M. (2012) Excitonic transport in ZnO. *J. Mater. Res.*, **27** (17), 2225–2231.

#### Acknowledgement:

The authors would like to thank Katie McBean, Geoff McCredie and Dr. Angus Gentle for the technical support at UTS, and Dr. Marie Wintrebert-Fouquet for her assistance with the Hall effect measurements at BluGlass Australia.

This research work was financially supported by the Australian Research Council, Discovery Program Scheme, Discovery Project DP150103317.